ACS APPLIED MATERIALS & INTERFACES

Research Article

www.acsami.org

Facile Hydrothermal Synthesis and Surface Functionalization of Polyethyleneimine-Coated Iron Oxide Nanoparticles for Biomedical Applications

Hongdong Cai,[†] Xiao An,[‡] Jun Cui,[§] Jingchao Li,[§] Shihui Wen,[§] Kangan Li,[‡] Mingwu Shen,*[,§] Linfeng Zheng,[‡] Guixiang Zhang,*[,‡] and Xiangyang Shi*[,†,§,⊥]

[†]State Key Laboratory for Modification of Chemical Fibers and Polymer Materials and [§]College of Chemistry, Chemical Engineering and Biotechnology, Donghua University, Shanghai 201620, People's Republic of China

[‡]Department of Radiology, Shanghai First People's Hospital, School of Medicine, Shanghai Jiaotong University, Shanghai 200080, People's Republic of China

[⊥]CQM-Centro de Química da Madeira, Universidade da Madeira, Campus da Penteada, 9000-390 Funchal, Portugal

Supporting Information

ABSTRACT: We report the facile hydrothermal synthesis and surface functionalization of branched polyethyleneimine (PEI)-coated iron oxide nanoparticles (Fe_3O_4–PEI NPs) for biomedical applications. In this study, Fe_3O_4–PEI NPs were synthesized via a one-pot hydrothermal method in the presence of PEI. The formed Fe_3O_4–PEI NPs with primary amine groups on the surface were able to be further functionalized with polyethylene glycol (PEG), acetic anhydride, and succinic anhydride, respectively. The formed pristine and functionalized Fe_3O_4–PEI NPs were characterized via different techniques. We showed that the sizes of the Fe_3O_4–PEI NPs were able to be controlled by varying the mass ratio of Fe(II) salt and PEI. In addition, the formed Fe_3O_4–PEI NPs with different surface functionalities had good water dispersibility, colloidal stability, and relatively high R_2 relaxivity (130–160 1/(mM·s)). Cell viability assay data revealed that the surface PEGylation and acylation of Fe_3O_4–PEI NPs rendered them with good biocompatibility in the given concentration range, while the pristine aminated Fe_3O_4–PEI NPs started to display slight toxicity at the concentration of 50 μg/mL. Importantly, macrophage cellular uptake results demonstrated that both PEGylation and acetylation of Fe_3O_4–PEI NPs were able to significantly reduce the nonspecific macrophage uptake, likely rendering the particles with prolonged circulation time. With the proven hemocompatibility and rich amine conjugation chemistry, the Fe_3O_4–PEI NPs with different surface functionalities may be applied for various biomedical applications, especially for magnetic resonance imaging and therapy.

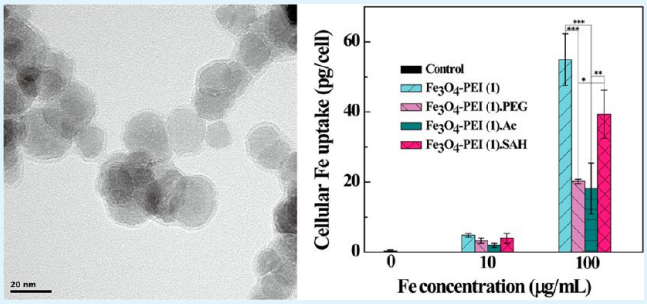

KEYWORDS: *iron oxide nanoparticles, polyethyleneimine, hydrothermal synthesis, biocompatibility, macrophage cellular uptake*

INTRODUCTION

Magnetic iron oxide nanoparticles (Fe_3O_4 NPs) have been extensively used for various biomedical applications including cell[1] and protein[2] separation, drug[3] and gene[4] delivery, hyperthermia,[5] and magnetic resonance (MR) imaging.[6−10] To be successfully utilized for biomedical applications, the Fe_3O_4 NPs are generally required to be colloidally stable, to have reduced nonspecific uptake by reticuloendothelial system (RES), or to have active targeting specificity after functionalized with targeting ligands. Surface modification with hydrophilic and/or biocompatible polymers on the surface of Fe_3O_4 NPs has been reported to be an effective and important strategy to make the particles meet the above requirements. Various polymers such as albumin,[11] dextran,[11−14] dendrimers,[6,7,15−18] polyethylene glycol (PEG),[19−21] or polyethyleneimine (PEI)[22−25] have been coated onto Fe_3O_4 NP surfaces to improve their stability or/and decrease the uptake by the RES. Although the reported polymer-coated Fe_3O_4 NPs are able to improve the biomedical performances required for the specific applications, development of a versatile and multifunctional Fe_3O_4 NP system with tunable surface modifications for various applications still maintains a great challenge.

Branched polyethyleneimine (PEI) possesses a high density of primary amino groups.[26,27] This enables PEI to be used as a stabilizer to form inorganic NPs, such as gold NPs.[28−30] Likewise, as reported in the literature, PEI-modified Fe_3O_4 NPs[22,31] or multiwalled carbon nanotubes (MWCNTs)[32,33] can be further functionalized via the active amine groups for

Received: November 28, 2012
Accepted: January 28, 2013
Published: February 6, 2013

Scheme 1. Schematic Illustration of the Hydrothermal Synthesis of Fe_3O_4–PEI NPs and the Subsequent Functionalization of the Fe_3O_4–PEI NPs

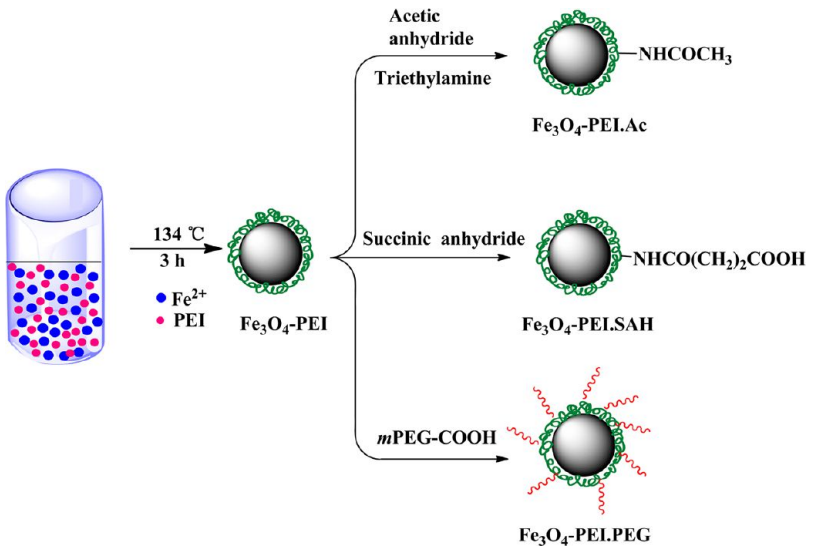

Table 1. Fe_3O_4–PEI NPs Synthesized under Different Reaction Conditions

product	$FeCl_2{\cdot}4H_2O$ (g)	H_2O (mL)	$NH_3{\cdot}H_2O$ (mL)	PEI (g)	yield[a](%)	diameter[b] (nm)	diameter[c] (nm)
Fe_3O_4–PEI (1)	1.25	7.75	6.25	0.54	79.62	11.5 ± 3.40	11.5
Fe_3O_4–PEI (2)	0.25	12.75	1.25	0.05	92.33	20.2 ± 5.99	17.5
Fe_3O_4–PEI (3)	0.25	12.75	1.25	0.10	75.78	16.7 ± 4.83	18.3
Fe_3O_4–PEI (4)	0.25	12.75	1.25	0.22	69.07	21.8 ± 6.47	18.9

[a]Calculated by dividing the initial Fe molar amount of the $FeCl_2{\cdot}4H_2O$ by that of Fe_3O_4–PEI NPs. [b]Measured by TEM. [c]Measured by XRD.

different biomedical applications. In general, the amine groups of PEI or PEI-modified NPs often give rise to severe cytotoxicity and nonspecific cell membrane binding,[34] which is not desirable for most of the biological applications. Neutralization of the surface amine groups to decrease the positive surface potential of the particles has been generally used to overcome the above drawbacks. For example, the primary amine groups of PEI-modified MWCNTs can be acetylated or carboxylated to significantly improve the materials' biocompatibility.[32] Similarly, PEGylation of the amino groups of biomaterials is another strategy to improve the materials' biocompatibility and prolong their blood circulation times.[35−37] For example, PEGylated dendrimers have been used as templates to synthesize dendrimer-entrapped gold NPs with significantly improved biocompatibility for in vivo computed tomography imaging applications.[38,39]

In our previous work, we applied a one-pot hydrothermal approach to successfully synthesize water-dispersible and colloidally stable 3-aminopropyltrimethoxysilane (APTS)-coated Fe_3O_4 NPs (Fe_3O_4@APTS). The aminated Fe_3O_4@APTS NPs were able to be further acetylated or carboxylated to significantly improve the biocompatibility of the particles.[40] This prior success leads us to hypothesize that PEI-coated Fe_3O_4 NPs may also be formed via the facile hydrothermal approach and the PEI-coated Fe_3O_4 NPs may also be further functionalized to improve their biocompatibility or decrease the macrophage cellular uptake.

In this present study, we synthesized PEI-coated Fe_3O_4 NPs (for short, Fe_3O_4–PEI NPs) via a one-pot hydrothermal method using PEI as stabilizer. The amine groups of the formed Fe_3O_4–PEI NPs were further functionalized with PEG, acetic anhydride, and succinic anhydride, respectively (Scheme 1). These formed pristine and functionalized Fe_3O_4–PEI NPs were characterized by X-ray diffraction (XRD), Fourier transform infrared spectrometry (FTIR), thermogravimetry analysis (TGA), transmission electron microscopy (TEM), dynamic light scattering (DLS), and zeta potential measurements. T_2 relaxation rate of the Fe_3O_4–PEI NPs was measured using a magnetic resonance imaging system. 3-(4,5-Dimethylthiazol-2-yl)-2,5-diphenyltetrazolium bromide (MTT) cell viability and hemolysis assay were used to assess the cytotoxicity and hemocompatibility of the particles, respectively. The cellular uptake of Fe_3O_4–PEI NPs with different functionalities by macrophage cells (Raw 264.7 cells) was determined by inductively coupled plasma-atomic emission spectroscopy (ICP-AES). To our best knowledge, this is the first report related to the facile one-step synthesis of PEI-coated Fe_3O_4 NPs with surface reactive amines and the further modification of aminated Fe_3O_4–PEI NPs for biomedical applications.

EXPERIMENTAL SECTION

Materials. All chemicals were of analytical grade from commercial sources and used without further purification. PEG monomethyl ether with one end of carboxyl group (*m*PEG-COOH) was from Shanghai Yanyi Biotechnology Corporation (Shanghai, China). Ferrous chloride tetrahydrate ($FeCl_2{\cdot}4H_2O$ > 99%), ammonia (25−28% NH_3 in water solution), triethylamine, acetic anhydride, dimethyl sulfoxide (DMSO), 1-ethyl-3-(3-dimethylaminopropyl) carbodiimide hydrochloride (EDC), potassium ferrocyanide, hydrochloric acid, branched PEI (M_w = 25 000), and all the other chemicals and solvents were purchased from Aldrich (St. Louis, MO). KB cells (a human epithelial carcinoma cell line) and Raw 264.7 cells (a type of mouse macrophage cell line) were from Institute of Biochemistry and Cell Biology, the Chinese Academy of Sciences (Shanghai, China). RPMI 1640 medium, Dulbecco's modified eagle's medium (DMEM), fetal bovine

dx.doi.org/10.1021/am302883m | ACS Appl. Mater. Interfaces 2013, 5, 1722−1731

serum (FBS), penicillin, and streptomycin were purchased from Gibco (UK). 3-(4,5-Dimethylthiazol-2-yl)-2,5-diphenyltetrazolium bromide (MTT) was acquired from Shanghai Sangon Biological Engineering Technology & Services Co., Ltd. (Shanghai, China). Water used in all experiments was purified using a Milli-Q Plus 185 water purification system (Millipore, Bedford, MA) with resistivity higher than 18.2 MΩ·cm.

Synthesis of Fe_3O_4–PEI NPs. A series of Fe_3O_4–PEI NPs with tunable sizes were synthesized using a hydrothermal approach described in our previous work with slight modification.[40,41] The sizes of Fe_3O_4–PEI NPs were tailored by using different feed ratios of reactants (Table 1). In a typical synthesis (e.g., Fe_3O_4–PEI (1) in Table 1), $FeCl_2{\cdot}4H_2O$ (1.25 g) was first dissolved in 7.75 mL water. Under vigorous stirring, ammonium hydroxide (6.25 mL) was added, and the suspension was continuously stirred in air for additional 10 min, allowing the iron(II) to be oxidized. Then, the reaction mixture was transferred to an autoclave with a volume of 50 mL (KH-50 autoclave, Shanghai Yuying Instrument Co., Ltd., Shanghai) and 5 mL aqueous solution containing 0.54 g PEI was added into the autoclave. After being stirred thoroughly, the reaction mixture was autoclaved at 134 °C with a gauge pressure of 2 bar. After 3 h reaction, the mixture was cooled down to room temperature. The black precipitate was collected by magnetic separation and purified with water 5 times to remove excess reactants and byproducts. Finally, the obtained Fe_3O_4–PEI NPs were redispersed in water.

Functionalization of Fe_3O_4–PEI NPs. The amine groups on the surface of the Fe_3O_4–PEI NPs were further PEGylated, acetylated, and carboxylated by reacting with *m*PEG-COOH, acetic anhydride, and succinic anhydride, respectively, according to some of the protocols described in our previous work.[38,40] To form Fe_3O_4–PEI·PEG NPs, Fe_3O_4–PEI NPs were modified with *m*PEG-COOH at a molar ratio of the PEI amine groups on the Fe_3O_4–PEI NPs to *m*PEG-COOH of 5:1 (Table 2). Typically, EDC (23.00 mg) and *m*PEG-COOH (22.03 mg)

Table 2. Synthesis Conditions and the Diameters of Fe_3O_4–PEI·PEG NPs

product	Fe_3O_4–PEI (g)	*m*PEG-COOH (g)	EDC (g)	NP diameter (nm)[a]
Fe_3O_4–PEI (1)·PEG	Fe_3O_4–PEI (1), 24.44 g	22.03	23.00	12.0 ± 3.26
Fe_3O_4–PEI (3)·PEG	Fe_3O_4–PEI (3), 6.04 g	4.124	6.82	18.7 ± 6.09

[a]Measured by TEM.

were added into 5 mL DMSO and the mixture solution was stirred for 3 h to activate the carboxylic acid group of *m*PEG-COOH. The activated *m*PEG-COOH solution was then added to 2 mL aqueous solution containing 24.44 mg Fe_3O_4–PEI NPs (Fe_3O_4–PEI (1) in Table 1), and the mixture solution was allowed to react for 3 d with shaking. Thereafter, the PEGylated Fe_3O_4–PEI NPs were collected by magnetic separation and purified with water for 5 times to remove excess reactants and byproducts. Finally, the obtained Fe_3O_4–PEI·PEG NPs (Fe_3O_4–PEI (1)·PEG in Table 2) were dispersed in water.

The Fe_3O_4–PEI NPs were acetylated to neutralize the positive surface charge of the particles with a reactant molar ratio of 5:5:1 (triethylamine:acetic anhydride:the amino groups of Fe_3O_4–PEI NPs). Typically, 80 μL triethylamine was first added to 2 mL aqueous solution containing 24.44 mg Fe_3O_4–PEI NPs (Fe_3O_4–PEI (1) in Table 1) and the solution was thoroughly mixed for 30 min. Then, acetic anhydride (60 μL) was dropwise added into the Fe_3O_4–PEI/triethylamine mixture solution under vigorous stirring. The mixture was allowed to react for 48 h. Thereafter, the excess reactants and byproduct were removed by 5 cycles of magnetic separation/washing/dispersion in water to obtain the final product of Fe_3O_4–PEI (1)·Ac NPs, which were finally dispersed in water.

Similarly, the Fe_3O_4–PEI NPs were also functionlized by carboxylating the surface amines of the Fe_3O_4–PEI NPs with succinic anhydride using a reactant molar ratio of 5:1 (succinic anhydride:the amino groups of Fe_3O_4–PEI NPs). Briefly, 2 mL DMSO solution containing 24.44 mg Fe_3O_4–PEI NPs (Fe_3O_4–PEI (1) in Table 1) was mixed with 4 mL of DMSO solution containing 27.7 mg succinic anhydride under vigorous stirring. The mixture was allowed to react for 48 h, and the excess reactants and byproduct were then removed by five cycles of magnetic separation/washing/redispersion in water to obtain the Fe_3O_4–PEI (1)·SAH NPs, which were finally dispersed in water.

Characterization Techniques. To characterize the crystalline structure and the size of the products, XRD was performed using a D/max 2550 PC X-ray diffractometer (Rigaku Corporation, Japan) with Cu Kα radiation (λ = 0.154 nm) at 40 kV and 200 mA. The scan range (2θ) was from 15° to 80°. The size and morphology of the formed Fe_3O_4–PEI and Fe_3O_4–PEI·PEG NPs were confirmed by TEM imaging using a JEOL 2010F analytical electron microscope operating at 200 kV. TEM samples were prepared by placing one drop of diluted particle suspension (5 μL) onto a carbon-coated copper grid, and the suspension was air-dried before measurements. The diameters of the formed NPs were measured using image analysis software ImageJ 1.40G (http://rsb.info.nih.gov/ij/download.html). At least 200 randomly selected NPs in different TEM images for each sample were analyzed to acquire the size distribution histogram. FTIR spectra were collected using a Nicolet Nexus 670 FTIR spectrometer (Thermo Nicolet Corporation, USA). Dry particles were mixed with grounded KBr crystals, and the samples were pressed as pellets before measurements. TGA was carried out using a TG 209 F1 (NETZSCH Instruments Co., Ltd., Germany) thermogravimetric analyzer with a heating rate of 20 °C/min and a temperature range of 30–650 °C under nitrogen atmosphere. Zeta potential of the pristine and functionalized Fe_3O_4–PEI NPs was measured using a Malvern Zetasizer Nano ZS model ZEN3600 (Worcestershire, UK) equipped with a standard 633 nm laser. The hydrodynamic size of the formed NPs dispersed in water was also analyzed via DLS using the above Zetasizer Nano ZS system. In addition, to assess the colloidal stability of the different NPs dispersed in PBS buffer or the RPMI 1640 cell culture medium over different time periods (up to 8 d), the change of their hydrodynamic sizes was also monitored via DLS. Finally, the colloidal stability of the formed pristine and functionalized Fe_3O_4–PEI NPs in different media including water, phosphate buffer saline (PBS), or cell culture medium was also visually assessed for a period of time up to one month.

The Fe concentration of the Fe_3O_4–PEI NPs before and after surface modification was determined by a Leeman Prodigy ICP-AES system (Hudson, NH03051, USA). T_2 relaxometry of the NPs was performed using a 3.0 T Signa HDxt superconductor magnetic resonance system (GE Medical Systems, Milwaukee, WI, USA) with a wrist receiver coil. The aqueous solutions of NPs (2 mL) with Fe concentrations of 0.002–0.02 mM were transferred into 2-mL Eppendorf tubes. T_2 relaxation times were then measured using a MFSE sequence. A total of eight echoes were used with the following parameters: TR = 500 ms, TE = 21.9/Ef, flip angle = 90°, resolution = 256 × 256, section thickness = 2 mm, and FOV = 80 mm × 80 mm. The T_2 mapping was performed on a workstation running with Functool 4.5.3. (GE Medical Systems). The T_2 relaxivity (R_2) was calculated from a linear fit of $1/T_2$ as a function of the Fe concentration of the particles.

Cytotoxicity Assay. The KB cells were continuously grown in a 50-mL culture flask in regular RPMI 1640 medium supplemented with 10% heat-inactivated FBS, 100 U/mL penicillin, and 100 U/mL streptomycin. MTT assay was used to quantify the viability of the cells treated by Fe_3O_4–PEI NPs with different functionalities. In brief, 1×10^4 KB cells were seeded into each well of a 96-well cell culture plate. After overnight incubation to bring the cells to 80% confluence, the medium was replaced with fresh medium containing the NPs at different particle concentrations (0, 10, 25, 50, and 100 μg/mL, respectively). After 24 h incubation at 37 °C and 5% CO_2, MTT in PBS buffer was added to each well to detect the metabolically active cells. The assays were carried out according to the manufacturer's instructions and the absorbance of each well was measured using a

Thermo Scientific Multiskan MK3 ELISA reader (Thermo Scientific, USA) at 570 nm. Mean and standard deviation for the triplicate wells were reported. After treatment with the functionalized Fe_3O_4 NPs for 24 h, the cell morphology was observed by Leica DM IL LED inverted phase contrast microscope (Leica, Germany). The magnification was set at 200× for all samples.

Hemolysis Assay. Fresh human blood stabilized with heparin was kindly provided by Shanghai First People's Hospital (Shanghai, China). Healthy red blood cells (HRBCs) for hemolysis assay were pretreated and collected according to the procedures described in the literature.[9] Briefly, HRBCs was isolated from fresh human blood by centrifugation at 2000 rpm for 10 min and purified by successively washing with PBS buffer for 5 times. Thereafter, the HRBCs were diluted 10 times with PBS buffer. The diluted HRBC suspension (0.1 mL) was added to 0.9 mL water (positive control), 0.9 mL PBS (negative control), and 0.9 mL PBS buffer containing Fe_3O_4–PEI (1), Fe_3O_4–PEI (1)·PEG, Fe_3O_4–PEI (1)·Ac, and Fe_3O_4–PEI (1)·SAH NPs, respectively, with a concentration ranging from 50 to 400 μg/mL. After a gentle shaking, the mixtures were kept still for 2 h at room temperature. Then, after centrifugation of the mixture (10 000 rpm, 1 min), the photos of the mixtures were taken and the absorbance of the supernatants (hemoglobin) was measured by Lambda 25 UV–vis spectrophotometer (Perkin-Elmer, U.S.A.). The hemolysis percentages of the samples were calculated by dividing the difference in absorbances at 541 nm between the sample and the negative control by the difference in absorbances at 541 nm between positive and negative controls.

Macrophage Cellular Uptake. Raw 264.7 cells, a type of mouse leukemic monocyte macrophage cell line, were continuously cultured in T25 cell culture flasks with DMEM supplemented with 10% heat-inactivated FBS, 100 U/mL penicillin, and 100 U/mL streptomycin. Briefly, 1×10^6 macrophage cells were seeded into each well of 24-well plates and incubated with fresh medium containing differently functionalized Fe_3O_4–PEI NPs at different Fe concentrations (0, 10, and 100 μg/mL, respectively) for 4 h at 37 °C and 5% CO_2. Then, the growth medium was removed and the cells were washed with PBS buffer for 3 times, trypsinsized, and suspended in DMEM. The cell concentrations were determined by hemacytometry. After that, the cells were collected by centrifugation at 1000 rpm for 10 min and lysed using an aqua regia solution (0.5 mL) for 2 h. Finally the cellular Fe uptake was quantified by ICP-AES.

To qualitatively confirm the iron uptake by Raw 264.7 cells, Prussian blue staining of cells was performed. In brief, 5×10^5 cells were seeded into each well of 24-well cell culture plates. After overnight incubation at 37 °C and 5% CO_2 to bring the cells to 80% confluence, the medium was replaced with fresh medium containing differently functionalized Fe_3O_4–PEI NPs at an Fe concentration of 20 μg/mL. The cells were continuously incubated for 4 h. Then, the cells were washed 3 times with PBS, fixed with *p*-formaldehyde solution at 4 °C for 15 min, and stained with Prussian blue reagent (Potassium ferrocyanide (1 g) dissolved in water (9 mL) was mixed with 36–38% HCl (1 mL)) at 37 °C for 30 min. The cells were imaged by Leica DM IL LED inverted phase contrast microscope. The magnification was set at 400× for all samples.

Interaction of Differently Functionalized Fe_3O_4–PEI NPs with Protein. Differently functionalized Fe_3O_4–PEI NPs with different final concentrations (0, 25, and 50 μg/mL, respectively) were incubated with 1 mL FBS solution (10%, in PBS buffer) in a 24-well tissue culture plate for different time periods (4 and 24 h) at 37 °C. After that, each sample was collected and centrifuged (12000 rpm, 5 min), and the content of FBS in the supernatant was quantified using a Lambda 25 UV–vis spectrophotometer (Perkin-Elmer, USA) at 280 nm.

Statistical Analysis. A one-way analysis of variance (ANOVA) statistical method was performed to detect the cytotoxicity, cellular uptake, and protein adsorption differences between the differently functionalized Fe_3O_4–PEI NPs or between the samples and the control. The value 0.05 was selected as the statistical significance level, and the data were indicated with (*) for $p < 0.05$, (**) for $p < 0.01$, and (***) for $p < 0.001$, respectively.

RESULTS AND DISCUSSION

Synthesis of Fe_3O_4–PEI NPs. Hydrothermal approach has been proven to be effective and facile in the formation of magnetic iron oxide NPs.[40−42] Our previous work has shown that Fe_3O_4 NPs with controllable size and tunable magnetic properties are able to be formed via the hydrothermal strategy.[41] In our another work, APTS-coated Fe_3O_4 NPs can be hydrothermally synthesized in the presence of APTS, and the aminated APTS-coated Fe_3O_4 NPs are able to be further functionalized to improve the biocompatibility of the particles.[40] In this study, we attempted to use the same hydrothermal method to synthesize PEI-coated Fe_3O_4 NPs.

Our previous work has shown that the size of Fe_3O_4 NPs can be controlled by varying the feeding ratio of reactants.[41] In this work, we chose a high and a low concentration of $FeCl_2$ (1.25 and 0.25 g $FeCl_2{\cdot}4H_2O$, respectively) as the Fe source, and then changed the mass ratio of $FeCl_2$ to PEI as well as the volume ratio of H_2O to $NH_3{\cdot}H_2O$ to synthesize a series of Fe_3O_4–PEI NP products (Table 1). The yield of the formed Fe_3O_4–PEI NPs was in the range of 69–92%. Note that the mixture volume of H_2O and $NH_3{\cdot}H_2O$ in the autoclave was kept constant to ensure that a similar amount of oxygen was used for the oxidation of Fe (II) (Table 1).

The crystal structure and size of the formed Fe_3O_4–PEI NPs were characterized using XRD (Figure 1). It is clear that the

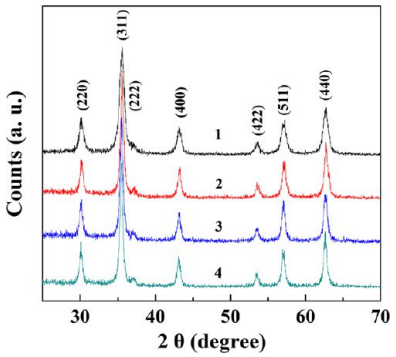

Figure 1. XRD patterns of Fe_3O_4–PEI NPs. 1, 2, 3, and 4 indicate the Fe_3O_4–PEI (1), Fe_3O_4–PEI (2), Fe_3O_4–PEI (3), and Fe_3O_4–PEI (4) NPs, respectively.

XRD patterns for all the formed Fe_3O_4–PEI NPs are identical, and the lattice spacings observed at 2θ of 30.1, 35.5, 37.1, 43.3, 53.6, 57.1, and 62.7° well match the [220], [311], [222], [400], [422], [511], and [440] planes of Fe_3O_4 crystals, respectively, in agreement with those reported in our previous work.[40,41] The mean diameters of the Fe_3O_4–PEI NPs formed under different conditions were calculated based on the major diffraction peak (plane [311]) according to the Debye–Scherrer equation (Table 1). Obviously, the concentration of $FeCl_2$ appreciably impacted the size of the NPs, similar to that reported in our previous work.[41] The diameter of Fe_3O_4–PEI (1) NPs synthesized using 1.25 g $FeCl_2{\cdot}4H_2O$ was much smaller than those of the other Fe_3O_4–PEI NPs formed using 0.25 g $FeCl_2.4H_2O$ as the Fe source (Fe_3O_4–PEI (2), Fe_3O_4–PEI (3), and Fe_3O_4–PEI (4)). When the amount of $FeCl_2{\cdot}4H_2O$ was fixed, the mass ratio of $FeCl_2{\cdot}4H_2O$/PEI did not seem to cause significant changes in the size of Fe_3O_4–PEI NPs (Fe_3O_4–PEI (2), Fe_3O_4–PEI (3) and Fe_3O_4–PEI (4)). These XRD results reveal that the particles are highly crystalline

dx.doi.org/10.1021/am302883m | ACS Appl. Mater. Interfaces 2013, 5, 1722–1731

and the diameters of the Fe_3O_4–PEI NPs can be controlled in the range of 11.5–18.9 nm under the experimental conditions.

The morphology and size of the formed Fe_3O_4–PEI NPs were investigated by TEM (Figure 2). It can be clearly seen that

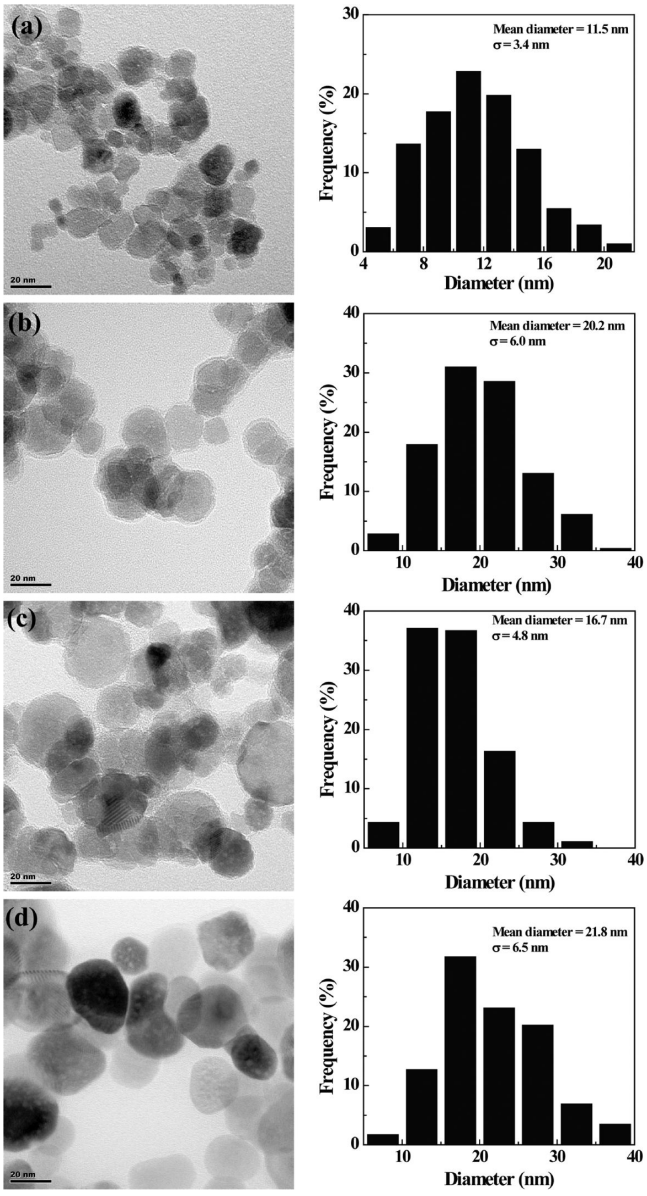

Figure 2. TEM micrographs and size distribution histograms of (a) Fe_3O_4–PEI (1), (b) Fe_3O_4–PEI (2), (c) Fe_3O_4–PEI (3), and (d) Fe_3O_4–PEI (4) NPs.

the particles with a spherical or quasi-spherical shape are surrounded with a transparent polymer shell on the outer surface of the NPs, confirming the successful coating of PEI. Compared to the naked Fe_3O_4 NPs having a mean size of 31.1 nm prepared under the same conditions in the absence of PEI,[41] the size of Fe_3O_4–PEI NPs dropped significantly with a size range of 16.7–21.8 nm depending on the added amount of PEI during the synthesis process (Figure 2b–d). This suggests that the nucleation and crystal growth of Fe_3O_4 NPs are able to be limited by the PEI. In addition, compared to APTS-coated Fe_3O_4 NPs with a mean size of 6.5 nm prepared under the same conditions in the presence of APTS,[40] Fe_3O_4–PEI (1) NPs have a larger size of 11.5 nm (Figure 2a), presumably due to the fact that APTS-assisted silanization is more powerful in limiting the growth of the NPs. The TEM results also show that the added amount of $FeCl_2$ under similar conditions appreciably impacts the size of the synthesized NPs. A higher amount of $FeCl_2{\cdot}4H_2O$ led to the formation of NPs with a smaller mean diameter (Table 1, Fe_3O_4–PEI (1) NPs with a diameter of 11.5 nm, and Fe_3O_4–PEI (2–4) NPs with diameters ranging from 16.7 to 21.8 nm, respectively), corroborating the XRD results (Figure 1).

The PEI coating on the Fe_3O_4–PEI NPs was also qualitatively verified by FTIR spectrometry (Figure 3). The

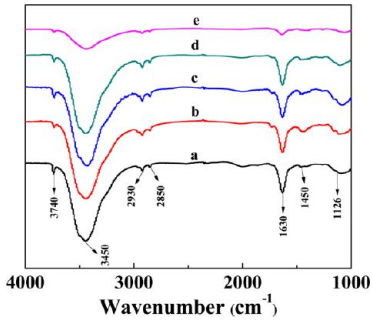

Figure 3. FTIR spectra of NPs of (a) Fe_3O_4–PEI (1), (b) Fe_3O_4–PEI (2), (c) Fe_3O_4–PEI (3), (d) Fe_3O_4–PEI (4), and (e) naked Fe_3O_4 NPs synthesized by the hydrothermal approach in the absence of PEI.

stronger absorption bands at 3450 and 1630 cm^{-1} in the spectra of all Fe_3O_4–PEI NPs (Figure 3 curves a–d) could be attributed to the $—NH_2$ groups introduced from PEI. In contrast, uncoated Fe_3O_4 NPs display weak absorption bands at 3433 and 1630 cm^{-1}, which may be assigned to the O–H stretching and bending vibrations of physically adsorbed H_2O and the surface –OH groups of the NPs (Figure 3, curve e). The stronger absorption bands at 2930 and 2850 cm^{-1} for all Fe_3O_4–PEI NPs could be attributed to the $–CH_2–$ groups of PEI and the band at 1126 cm^{-1} is due to the stretching vibration of C–N bond. The FTIR spectroscopic results qualitatively confirmed the successful coating of PEI on the surface of Fe_3O_4 NPs.

To quantify the coating percentage of PEI on the surface of Fe_3O_4 NPs, TGA analysis was performed (Figure 4). It can be seen that the Fe_3O_4–PEI NPs have weight losses ranging from 7.34% to 9.69% when compared with the naked Fe_3O_4 NPs,

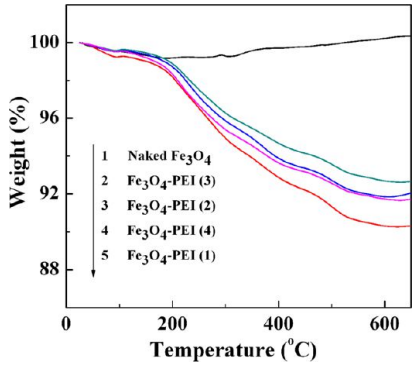

Figure 4. TGA curves of the naked Fe_3O_4 NPs and Fe_3O_4–PEI NPs. 1, 2, 3, 4, and 5 indicate the naked Fe_3O_4 NPs, Fe_3O_4–PEI (3), Fe_3O_4–PEI (2), Fe_3O_4–PEI (4), and Fe_3O_4–PEI (1) NPs, respectively.

indicative of the successful PEI coating onto the surface of Fe_3O_4 NPs.

Functionalization of Fe_3O_4–PEI NPs. The surface amine groups of the formed Fe_3O_4–PEI NPs were PEGylated (Table 2), acetylated, and carboxylated (Table 3) by reacting with *m*PEG-COOH, acetic anhydride, and succinic anhydride, respectively, to generate Fe_3O_4–PEI NPs with different surface functionalities (Scheme 1).

Table 3. Zeta Potential and Hydrodynamic Size of Fe_3O_4–PEI (1), Fe_3O_4–PEI (1)·Ac, Fe_3O_4–PEI (1)·SAH, and Fe_3O_4–PEI (1)·PEG NPs

sample	zeta potential value (mV)	hydrodynamic size (nm)	polydispersity index (PDI)
Fe_3O_4–PEI (1)	38.1 ± 0.15	310.4 ± 3.40	0.40 ± 0.015
Fe_3O_4–PEI (1)·Ac	26.8 ± 0.20	161.8 ± 35.13	0.65 ± 0.126
Fe_3O_4–PEI (1)·SAH	−17.3 ± 0.35	217.6 ± 2.87	0.28 ± 0.016
Fe_3O_4–PEI (1)·PEG	30.9 ± 0.25	161.9 ± 4.16	0.21 ± 0.015

To confirm the modification of PEG on the surface of Fe_3O_4–PEI NPs, the weight loss of Fe_3O_4–PEI·PEG NPs was measured via TGA (Figure S1, Supporting Information). The Fe_3O_4–PEI (1) and Fe_3O_4–PEI (3) with different sizes were PEGylated. The weight loss of Fe_3O_4–PEI (1)·PEG and Fe_3O_4–PEI (3)·PEG was estimated to be 14.87% (Figure S1a) and 10.70% (Figure S1b), respectively. After subtracting the weight loss of Fe_3O_4–PEI (1) (9.69%, Figure 4) and Fe_3O_4–PEI (3) (7.34%, Figure 4), the amount of the modified PEG onto the Fe_3O_4–PEI (1)·PEG and Fe_3O_4–PEI (3)·PEG NPs was estimated to be 5.18% and 3.36%, respectively.

The morphology and size of the formed Fe_3O_4–PEI·PEG NPs were investigated by TEM (Figure 5). It is clear that the transparent shell of the Fe_3O_4–PEI·PEG NPs becomes slightly thicker than that of the corresponding NPs before PEGylation. In addition, the PEGylation modification led to the increase of

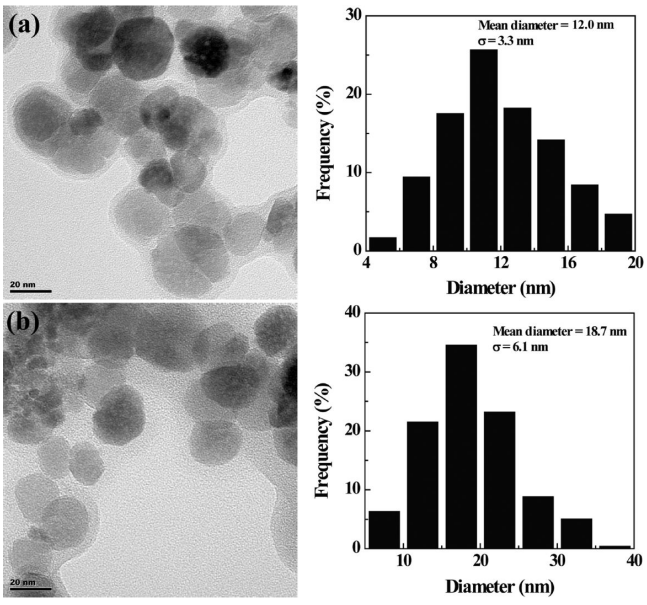

Figure 5. TEM micrographs and size distribution histograms of (a) Fe_3O_4–PEI (1)·PEG and (b) Fe_3O_4–PEI (3)·PEG NPs.

the sizes of the NPs: the mean diameter of Fe_3O_4–PEI (1)·PEG was increased from 11.5 nm (Fe_3O_4–PEI (1) NPs) to 12 nm, while the mean diameter of Fe_3O_4–PEI (3)·PEG NPs was increased from 16.7 nm (Fe_3O_4–PEI (3) NPs) to 18.7 nm. Both TGA and TEM results confirmed the successful PEGylation modification of the Fe_3O_4–PEI NPs.

Besides the PEGylation of Fe_3O_4–PEI NPs, we were also able to convert the surface PEI amines of Fe_3O_4–PEI NPs to acetyl and carboxyl groups (Scheme 1), similar to our previous work related to acylation of PEI-modified MWCNTs.[32] Zeta potential measurements were employed to confirm the surface potential alteration before and after surface modification. It can be seen that the surface potential of the positively charged aminated Fe_3O_4–PEI (1) NPs (+38.1 mV) is decreased to +26.8 mV after acetylation of the PEI amines (Fe_3O_4–PEI (1)·Ac NPs). It seems that the acetylation reaction is not able to completely shield the positive surface potential of the Fe_3O_4–PEI (1) NPs despite the use of excessive acetic anhydride. This is likely attributed to the fact that a portion of the PEI amines used to stabilize the Fe_3O_4 NPs via strong physical interaction is not able to be completely acetylated. Since most of the outer surface amines of the particles have been acetylated, the formed Fe_3O_4–PEI (1)·Ac NPs did not show the similar cytotoxicity to the Fe_3O_4–PEI (1) NPs without modification (see below). In contrast, the carboxylation reaction was able to shift the positive surface potential of the Fe_3O_4–PEI (1) NPs to negative (−17.3 mV). In addition, when a portion of PEI amines of Fe_3O_4–PEI (1) NPs was PEGylated, the surface potential of PEGylated Fe_3O_4–PEI (1)·PEG NPs was decreased to +30.9 from +38.1 mV (Table 3). Although the PEGylation modification is not able to completely neutralize the Fe_3O_4–PEI (1) NPs due to the less molar ratio between PEG and PEI amines, the modified PEG moieties are able to efficiently shield the electrostatic interaction between the particles and the cell membranes, leading to the improved biocompatibility of the particles (see below).

The hydrodynamic size of the Fe_3O_4–PEI (1) NPs in water before and after different modifications was analyzed with DLS (Table 3). It can be seen that the acetylation, carboxylation, and PEGylation modifications are able to significantly reduce the hydrodynamic size of the Fe_3O_4–PEI (1) NPs (310.4 nm) to 161.8, 217.6, and 161.9 nm, respectively (Table 3). It is worth noting that the measured hydrodynamic sizes of the particles are all larger than those measured by TEM. This should be due to the fact that DLS measures the aggregated clusters of the NPs in aqueous solution, while TEM measured the single NPs in a dry state, in agreement with our previous results.[9,43,44] The stability of all the Fe_3O_4–PEI NPs with different surface functionalities was evaluated by occasionally checking the hydrodynamic size change at a time period of one month. We show that the sizes of all the particles do not have appreciable changes, indicating that all the particles are colloidally stable in water.

The colloidal stability of Fe_3O_4–PEI NPs with different surface functional groups dispersed in PBS buffer or cell culture medium was also assessed over different time periods (up to 8 d) by monitoring the change of their hydrodynamic sizes via DLS (Figure S2 and Table S1, Supporting Information). It is clear that in both PBS buffer and cell culture medium, the hydrodynamic sizes of the Fe_3O_4–PEI NPs with different surface functional groups do not have appreciable changes, indicating their good colloid stability. It seems that the size

fluctuation of the particles dispersed in cell culture medium is much less than that dispersed in PBS buffer. Our results suggest that the noncovalent bonding of PEI on the surface of Fe_3O_4 NPs is able to render the good stability of the Fe_3O_4 NPs even after further functionalization of PEI with different chemical reactions. Furthermore, the colloidal stability of Fe_3O_4–PEI NPs with different surface functional groups dispersed in water, PBS buffer, or cell culture medium was visually confirmed over a period of one month. We show that all particles are colloidally stable and no precipitates were observed over the time period of at least one month (Figure S3, Supporting Information), which is essential for their biomedical applications.

T_2 Relaxivity of Fe_3O_4–PEI and Fe_3O_4–PEI·PEG NPs. With a good transverse relaxivity (R_2, the transverse relaxation rate per millimolar of iron), Fe_3O_4 NPs are known to be used as a T_2 negative contrast agent.[6,45] To explore the potential MR imaging ability, the T_2 of Fe_3O_4–PEI (1), Fe_3O_4–PEI (3), and their PEGylated counterparts was measured and the R_2 relaxivity was calculated (Figure 6). It can be seen that the

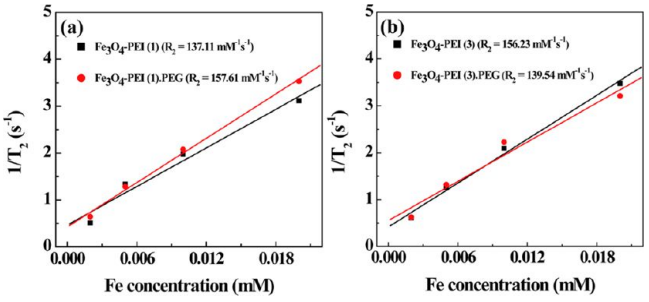

Figure 6. Linear fitting of $1/T_2$ of pristine and PEGylated (a) Fe_3O_4–PEI (1) NPs and (b) Fe_3O_4–PEI (3) NPs as a function of Fe concentration.

R_2 values of Fe_3O_4–PEI (1) and Fe_3O_4–PEI (3) were 137.11 and 156.23 1/(mM·s), respectively. After PEGylation, the R_2 of Fe_3O_4–PEI (1)·PEG and Fe_3O_4–PEI (3)·PEG was estimated to be 157.61 and 139.54 1/(mM·s), respectively. This suggests that partial PEGylation of Fe_3O_4–PEI NPs does not cause significant changes in the R_2 relaxivity of the particles and the formed Fe_3O_4–PEI and Fe_3O_4–PEI·PEG NPs may be potentially used as T_2 MR imaging contrast agents due to their good stability and relatively larger R_2 values when compared with APTS-coated Fe_3O_4 NPs[40] and Fe_3O_4 NPs coated with polyelectrolyte multilayers.[6]

Cytotoxicity of Fe_3O_4–PEI NPs with Different Surface Functionalities. Our previous studies have shown that the biocompatibility of aminated APTS-coated Fe_3O_4–PEI NPs[40] and PEI-modified MWCNTs[32] can be significantly improved by shielding the positive surface potential of the materials. In addition, PEGylation is also known to be a well-established strategy to improve the cytocompatbility of biomaterials.[36,38] We next explored the cytotoxicity of Fe_3O_4–PEI NPs with different surface functionalities. Phase contrast microscopic images show that at a relatively low particle concentration (e.g., 10 μg/mL), KB cells treated by all Fe_3O_4–PEI NPs with different surface functionalities are pretty healthy, similar to the PBS control (Figure S4, Supporting Information). Further quantitative MTT assay data (Figure 7) show that the viability of cells treated with Fe_3O_4–PEI (1)·PEG, Fe_3O_4–PEI (1)·Ac, or Fe_3O_4–PEI (1)·SAH NPs at the given concentrations (0–100 μg/mL) does not display a significantly statistical difference

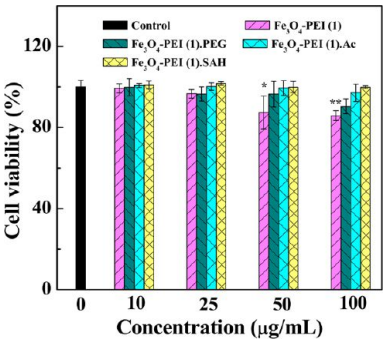

Figure 7. MTT assay of KB cell viability after treatment with PBS (control) and the pristine and functionalized Fe_3O_4–PEI (1) NPs at the particle concentration of 0–100 μg/mL for 24 h.

when compared with that of control cells treated with PBS buffer ($p > 0.05$). In contrast, Fe_3O_4–PEI (1) NPs started to display slight cytotoxicity at a concentration of 50 μg/mL ($p < 0.05$), suggesting that the aminated Fe_3O_4–PEI NPs are not favorable for cell growth at high concentrations. The slight cytotoxicity of the Fe_3O_4–PEI (1) NPs at high concentrations may be due to high positive surface potential of the particles, leading to strong electrostatic interaction with the negatively charged cell membranes, in agreement with our previous results.[32,40] The surface modifications via acetylation, carboxylation, or PEGylation appear to significantly shield the positive surface potential of the particles or the electrostatic interaction between the particles with the cell membranes, thereby leading to improved cytocompatibility of the particles at the concentration up to 100 μg/mL.

Hemolysis Assay. Hemocompatibility is of great importance for the biomaterials required to contact blood. In this study, hemolysis assay was used to investigate the hemocompatibility of the formed pristine and differently functionalized Fe_3O_4–PEI NPs. Figure 8 shows the UV–vis spectra and the photograph of HRBC suspension after treatment with Fe_3O_4–PEI (1) and Fe_3O_4–PEI (1)·PEG at different concentrations (from 50 to 400 μg/mL), respectively. The hemolysis pencentages of the samples were quantified based on the absorbance of the supernatant at 541 nm. It is apparent that even at a particle concentration of 400 μg/mL, the hemolysis percentages of Fe_3O_4–PEI (1), Fe_3O_4–PEI (1)·PEG, and Fe_3O_4–PEI (1)·Ac NPs (Figure S5a, Supporting Information) are all less than 5%, suggesting their excellent hemocompatibility. However, at the concentration of 400 μg/mL, Fe_3O_4–PEI (1)·SAH NPs (Figure S5b, Supporting Information) had a hemolysis pencentage of 7.65%. In contrast to the positive control (water), the pure PBS without NPs and PBS containing the pristine or differently functionalized Fe_3O_4–PEI NPs at different concentrations do not show visible hemolytic behavior (insets of Figure 8 and Figure S5). Therefore, the negligible hemolytic activity of the Fe_3O_4–PEI NPs with different surface modfications in a concentration range of 0–400 μg/mL along with their excellent cytocompatibility may enable them to be used for various biomedical applications.

Macrophage Uptake of Differently Functionalized Fe_3O_4–PEI NPs. For most of the biomedical applications of Fe_3O_4 NPs, the particles are generally required to be able to escape the macrophage uptake.[21] Surface modification of the particles is an effective strategy to decrease the macrophage uptake of the particles. After incubating these particles with the Raw 264.7 cells for 4 h at two different Fe concentrations (10

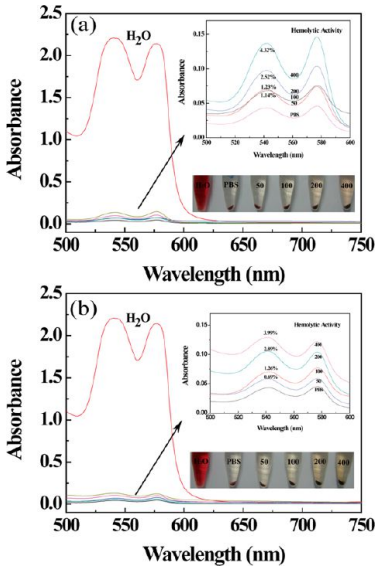

Figure 8. Hemolytical activity of Fe_3O_4–PEI (1) (a) and Fe_3O_4–PEI (1)·PEG (b) at different concentrations (50, 100, 200, and 400 μg/mL, respectively). PBS and water were used as negative and positive control, respectively. The bottom-right inset shows the photograph of HRBCs exposed to water, PBS, and PBS containing particles with different concentrations for 2 h, followed by centrifugation. The upper-right inset shows the enlarged UV–vis spectra shown in each panel.

μg/mL and 100 μg/mL), ICP-AES was used to assess the cellualr uptake of Fe element (Figure 9). Compared with the

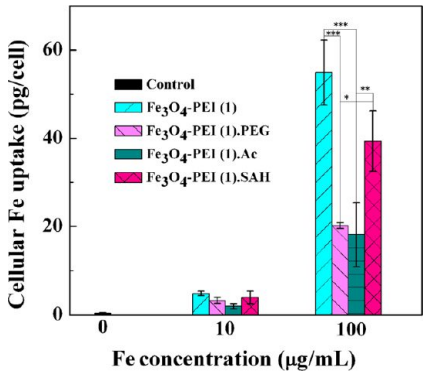

Figure 9. Macrophage uptake assay of pristine and functionalized Fe_3O_4–PEI (1) NPs with Fe concentration of 10 and 100 μg/mL.

control macrophage cells treated with PBS buffer, at the two tested Fe concentrations the macrophage cells treated with Fe_3O_4–PEI (1) NPs and Fe_3O_4–PEI (1)·SAH NPs showed the highest and the second highest uptake of Fe element, respectively, while the cells treated with Fe_3O_4–PEI (1)·PEG and Fe_3O_4–PEI (1)·Ac NPs showed much less Fe uptake, especially at the high Fe concentration ($p < 0.05$). In addtion, the Fe uptake by cells treated with all particles at the Fe concentration of 100 μg/mL is about 10 times higher than that treated with the corresponding particles at the Fe concentration of 10 μg/mL, indicating that the cellular Fe uptake is concentration-dependent, in agreement with previous report by Xie et al.[21] The approximately similar cellular uptake of Fe_3O_4–PEI (1)·PEG and Fe_3O_4–PEI (1)·Ac NPs suggests that both PEGylation and acetylation of the Fe_3O_4–PEI NPs are more or less equally efficient to reduce the nonspecific macrophage cellualr uptake of the particles, which is helpful for the particles to escape the RES.

The cellular iron uptake was further qualitatively confirmed by Prussian blue staining (Figure 10). Compared with the

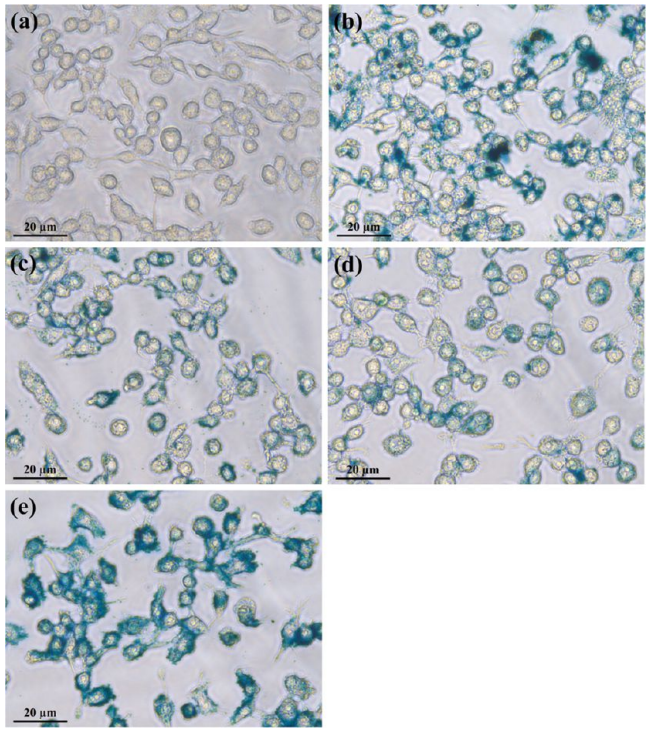

Figure 10. Phase contrast microscopic images of the macrophage cells (Raw 264.7 cells) after the Prussian blue staining. (a–e) Macrophage cells treated with PBS buffer (a), Fe_3O_4–PEI (1) (b), Fe_3O_4–PEI (1)·PEG (c), Fe_3O_4–PEI (1)·Ac (d), and Fe_3O_4–PEI (1)·SAH (e) NPs, respectively, with a particle concentration of 20 μg/mL for 4 h.

control cells treated with PBS that did not display the blue staining (Figure 10a), all the different Fe_3O_4–PEI NPs were able to be uptaken by the macrophage cells (Figure 10b–e). Apparently, the cells treated with Fe_3O_4–PEI (1) NPs and Fe_3O_4–PEI (1)·SAH NPs had much more blue staining than those treated with Fe_3O_4–PEI (1)·PEG and Fe_3O_4–PEI (1)·Ac NPs, corroborating the quantitative ICP-AES results.

Interaction of Differently Functionalized Fe_3O_4–PEI NPs with Protein. To explore the influence of the type of surface modification on the interaction of Fe_3O_4–PEI NPs with protein, the differently functionalized Fe_3O_4–PEI NPs were incubated with FBS solution for different time periods. We show that after incubation for 4 or 24 h at 37 °C, the protein level does not have any significant change for all the differently functionalized Fe_3O_4–PEI NPs ($p > 0.05$). This suggests that the prepared differently functionalized Fe_3O_4–PEI NPs do not have apparent protein absorption capacity (Figure S6, Supporting Information).

CONCLUSION

In summary, we have developed a facile approach to fabricating PEI-coated Fe_3O_4 NPs that can be further PEGylated, acetylated, or carboxylated to generate different surface functionalities. The size of the PEI-coated Fe_3O_4 NPs can be tuned within a range of 11–22 nm by varying the mass ratio of the reactants. The formed Fe_3O_4–PEI NPs with different

surface functionalities are water-soluble and colloidally stable and have relatively high R_2 relaxivity ranging from 130 to 160 1/(mM·s). In addition, the cytocompatibility of aminated Fe_3O_4–PEI NPs is able to be significantly improved after the surface modifcation with PEG moieties, acetyl groups, or carboxyl groups. Importantly, our results show that PEGylation and accelylation of Fe_3O_4–PEI NPs are able to significantly reduce the macrophage cellular uptake of the particles. With the good hemocompatibility and proven cytocompatibility in the given concentration range, the fabricated Fe_3O_4 NPs may be multifunctionalized for various biomedical applications, especially for targeted cancer imaging and therapeutics.

■ ASSOCIATED CONTENT

Supporting Information

Additional material characterization data. This information is available free of charge via the Internet at http://pubs.acs.org/.

■ AUTHOR INFORMATION

Corresponding Author

*E-mail: mwshen@dhu.edu.cn (M.S.); guixiangzhang@sina.com (G.Z.); or xshi@dhu.edu.cn (X.S.).

Notes

The authors declare no competing financial interest.

■ ACKNOWLEDGMENTS

This research is financially supported by the National Natural Science Foundation of China (81101150, 21273032, and 81271383), the Fund of the Science and Technology Commission of Shanghai Municipality (11 nm0506400 for X.S., 12520705500 for M.S., and 11JC1410500 for G.Z.), the Program for New Century Excellent Talents in University, State Education Ministry, and the Fundamental Research Funds for the Central Universities (for M.S. and X.S.). H.C. is thankful for the Innovation Funds of Donghua University Doctorate Dissertation of Excellence (BC201104). K.L. is thankful for the support from the Shanghai Natural Science Foundation (11ZR1429300) and the Songjiang Medical Climbing Program in Shanghai (2011PD04). X.S. gratefully acknowledges the Fundação para a Ciência e a Tecnologia (FCT) and Santander bank for the Invited Chair in Nanotechnology, and FCT through the Strategic Plan PEst-OE/QUI/UI0674/2011.

■ REFERENCES

(1) Liu, H. L.; Sonn, C. H.; Wu, J. H.; Lee, K. M.; Kim, Y. K. *Biomaterials* **2008**, *29*, 4003.
(2) Xie, H. Y.; Zhen, R.; Wang, B.; Feng, Y. J.; Chen, P.; Hao, J. *J. Phys. Chem. C* **2010**, *114*, 4825.
(3) Chen, Y.; Chen, H.; Zeng, D.; Tian, Y.; Chen, F.; Feng, J.; Shi, J. *ACS Nano* **2010**, *4*, 6001.
(4) Pan, B. F.; Cui, D. X.; Sheng, Y.; Ozkan, C. G.; Gao, F.; He, R.; Li, Q.; Xu, P.; Huang, T. *Cancer Res.* **2007**, *67*, 8156.
(5) Cheng, L.; Yang, K.; Li, Y.; Chen, J.; Wang, C.; Shao, M.; Lee, S. T.; Liu, Z. *Angew. Chem., Int. Ed.* **2011**, *50*, 7385.
(6) Shi, X.; Wang, S. H.; Swanson, S. D.; Ge, S.; Cao, Z.; Van Antwerp, M. E.; Landmark, K. J.; Baker, J. R., Jr. *Adv. Mater.* **2008**, *20*, 1671.
(7) Wang, S. H.; Shi, X.; Van Antwerp, M.; Cao, Z.; Swanson, S. D.; Bi, X.; Baker, J. R., Jr. *Adv. Funct. Mater.* **2007**, *17*, 3043.
(8) Yang, H.; Zhuang, Y.; Sun, Y.; Dai, A.; Shi, X.; Wu, D.; Li, F.; Hu, H.; Yang, S. *Biomaterials* **2011**, *32*, 4584.
(9) Cai, H.; Li, K.; Shen, M.; Wen, S.; Luo, Y.; Peng, C.; Zhang, G.; Shi, X. *J. Mater. Chem.* **2012**, *22*, 15110.
(10) Shen, M.; Shi, X. *Nanoscale* **2010**, *2*, 1596.
(11) Berry, C. C.; Wells, S.; Charles, S.; Curtis, A. S. G. *Biomaterials* **2003**, *24*, 4551.
(12) Berry, C. C.; Wells, S.; Charles, S.; Aitchison, G.; Curtis, A. S. G. *Biomaterials* **2004**, *25*, 5405.
(13) Moore, A.; Marecos, E.; Bogdanov, A.; Weissleder, R. *Radiology* **2000**, *214*, 568.
(14) Moore, A.; Weissleder, R.; Bogdanov, A. *J. Magn. Reson. Imaging* **1997**, *7*, 1140.
(15) Shi, X.; Thomas, T. P.; Myc, L. A.; Kotlyar, A.; Baker, J. R., Jr. *Phys. Chem. Chem. Phys.* **2007**, *9*, 5712.
(16) Bulte, J. W. M.; Douglas, T.; Witwer, B.; Zhang, S. C.; Strable, E.; Lewis, B. K.; Zywicke, H.; Miller, B.; van Gelderen, P.; Moskowitz, B. M.; Duncan, I. D.; Frank, J. A. *Nat. Biotechnol.* **2001**, *19*, 1141.
(17) Strable, E.; Bulte, J. W. M.; Moskowitz, B.; Vivekanandan, K.; Allen, M.; Douglas, T. *Chem. Mater.* **2001**, *13*, 2201.
(18) Chang, Y.; Liu, N.; Chen, L.; Meng, X.; Liu, Y.; Li, Y.; Wang, J. *J. Mater. Chem.* **2012**, *22*, 9594.
(19) Kohler, N.; Sun, C.; Fichtenholtz, A.; Gunn, J.; Fang, C.; Zhang, M. Q. *Small* **2006**, *2*, 785.
(20) Larsen, E. K. U.; Nielsen, T.; Wittenborn, T.; Birkedal, H.; Vorup-Jensen, T.; Jakobsen, M. H.; Ostergaard, L.; Horsman, M. R.; Besenbacher, F.; Howard, K. A.; Kjems, J. *ACS Nano* **2009**, *3*, 1947.
(21) Xie, J.; Xu, C.; Kohler, N.; Hou, Y.; Sun, S. *Adv. Mater.* **2007**, *19*, 3163.
(22) Chertok, B.; David, A. E.; Yang, V. C. *Biomaterials* **2010**, *31*, 6317.
(23) McBain, S. C.; Yiu, H. H. P.; El Haj, A.; Dobson, J. *J. Mater. Chem.* **2007**, *17*, 2561.
(24) Namgung, R.; Singha, K.; Yu, M. K.; Jon, S.; Kim, Y. S.; Ahn, Y.; Park, I. K.; Kim, W. J. *Biomaterials* **2010**, *31*, 4204.
(25) Masotti, A.; Pitta, A.; Ortaggi, G.; Corti, M.; Innocenti, C.; Lascialfari, A.; Marinone, M.; Marzola, P.; Daducci, A.; Sbarbati, A.; Micotti, E.; Orsini, F.; Poletti, G.; Sangregorio, C. *Magn. Reson. Mat. Phys. Biol. Med.* **2009**, *22*, 77.
(26) Jaeger, M.; Schubert, S.; Ochrimenko, S.; Fischer, D.; Schubert, U. S. *Chem. Soc. Rev.* **2012**, *41*, 4755.
(27) Neu, M.; Fischer, D.; Kissel, T. *J. Gene. Med.* **2005**, *7*, 992.
(28) Note, C.; Kosmella, S.; Koetz, J. *Colloid Surf. A–Physicochem. Eng. Asp.* **2006**, *290*, 150.
(29) Sun, X. P.; Dong, S. J.; Wang, E. K. *Polymer* **2004**, *45*, 2181.
(30) Wang, S. T.; Yan, J. C.; Chen, L. *Mater. Lett.* **2005**, *59*, 1383.
(31) Zhang, L.; Wang, T.; Li, L.; Wang, C.; Su, Z.; Li, J. *Chem. Commun.* **2012**, *48*, 8706.
(32) Shen, M.; Wang, S. H.; Shi, X.; Chen, X.; Huang, Q.; Petersen, E. J.; Pinto, R. A.; Baker, J. R., Jr.; Weber, W. J., Jr. *J. Phys. Chem. C* **2009**, *113*, 3150.
(33) Cao, X.; Chen, J.; Wen, S.; Peng, C.; Shen, M.; Shi, X. *Nanoscale* **2011**, *3*, 1741.
(34) Wen, S.; Zheng, F.; Shen, M.; Shi, X. *J. Appl. Polym. Sci.* **2012**, DOI: 10.1002/APP.38444.
(35) Veronese, F. M.; Mero, A. *Biodrugs* **2008**, *22*, 315.
(36) Otsuka, H.; Nagasaki, Y.; Kataoka, K. *Adv. Drug Delivery Rev.* **2003**, *55*, 403.
(37) Greenwald, R. B.; Choe, Y. H.; McGuire, J.; Conover, C. D. *Adv. Drug Delivery Rev.* **2003**, *55*, 217.
(38) Peng, C.; Zheng, L.; Chen, Q.; Shen, M.; Guo, R.; Wang, H.; Cao, X.; Zhang, G.; Shi, X. *Biomaterials* **2012**, *33*, 1107.
(39) Wen, S.; Li, K.; Cai, H.; Chen, Q.; Huang, Y.; Peng, C.; Shen, M.; Zhang, G.; Shi, X. *Biomaterials* **2013**, *34*, 1570.
(40) Shen, M.; Cai, H.; Wang, X.; Cao, X.; Li, K.; Wang, S. H.; Guo, R.; Zheng, L.; Zhang, G.; Shi, X. *Nanotechnology* **2012**, *23*, 105601.
(41) Ge, S.; Shi, X.; Sun, K.; Li, C.; Uher, C.; Baker, J. R., Jr.; Holl, M. M. B.; Orr, B. G. *J. Phys. Chem. C* **2009**, *113*, 13593.
(42) Daou, T. J.; Pourroy, G.; Begin-Colin, S.; Greneche, J. M.; Ulhaq-Bouillet, C.; Legare, P.; Bernhardt, P.; Leuvrey, C.; Rogez, G. *Chem. Mater.* **2006**, *18*, 4399.
(43) Liu, H.; Shen, M.; Zhao, J.; Guo, R.; Cao, X.; Zhang, G.; Shi, X. *Colloid Surf. B–Biointerfaces* **2012**, *94*, 58.

(44) Liu, H.; Sun, K.; Zhao, J.; Guo, R.; Shen, M.; Cao, X.; Zhang, G.; Shi, X. *Colloid Surf. A—Physicochem. Eng. Asp.* **2012**, *405*, 22.
(45) Villaraza, A. J. L.; Bumb, A.; Brechbiel, M. W. *Chem. Rev.* **2010**, *110*, 2921.

NOTE ADDED AFTER ASAP PUBLICATION

Due to a production error, this paper was published on the Web on February 19, 2013, with minor text errors. The corrected version was reposted on February 26, 2013.